Spine Anatomy Imaging
An Update

Amirali Modir Shanechi, MD[a,*], Matthew Kiczek, DO[a], Majid Khan, MBBS, MD[a], Gaurav Jindal, MD[b]

KEYWORDS

• Normal spinal anatomy • Spinal anatomy • Spinal MR imaging • Spinal CT • CT myelography

KEY POINTS

- MR imaging provides excellent detail of spinal anatomy including the intraspinal contents, neural foramina, joints, ligaments, intervertebral discs and bone marrow.
- CT better demonstrates the fine osseous detail of the spine and has an important role in the assessment of trauma as well as preoperative planning.
- CT myelography remains an alternative to MR imaging in those with contraindications or in the assessment of spinal CSF leak.
- This article illustrates normal spinal anatomy as defined by MR imaging and includes correlative CT and CT myelography images.

INTRODUCTION

Over the past few decades, spinal MR imaging has largely replaced computed tomography (CT) and CT myelography in the assessment of intraspinal pathologic conditions at institutions where MR imaging is available. Given its high-contrast resolution, MR imaging allows the differentiation of the several adjacent structures comprising the spine. Conventional CT remains a complementary imaging modality to MR imaging because of its high-resolution depiction of osseous anatomy and has a central role in operative planning or the evaluation of traumatic injury. CT myelography remains an alternative to MR imaging in those with contraindications to MR imaging or in the assessment of leak of cerebrospinal fluid (CSF) from the spine. This article illustrates normal spinal anatomy as defined by MR imaging, describes commonly used spinal MR imaging protocols (**Tables 1–3**), and discusses associated common artifacts. Correlative CT and CT myelography images are also included.

SPINAL MR IMAGING TECHNIQUES

Sagittal and axial MR images should be acquired through the cervical, thoracic, and lumbar segments of the spine, as they are generally considered complementary, and imaging the spine in only 1 plane may result in misinterpretation. The addition of coronal images may also be useful, especially in patients with scoliosis. Stacked axial images and/or angled images through the discs can be obtained, and are often useful when the indication for imaging is pain, degenerative change, and/or radiculopathy.[1] Although imaging in the axial plane is a matter of personal preference, using only angled axial images through the discs may be inadequate, because portions of the spinal canal will not be imaged axially. Slice thickness from 3 to 4 mm is generally optimal for

Disclosure: A.M. Shanechi and M. Kiczek have nothing to disclose. M. Khan is a consultant for Stryker Medical Corporation and Avecure Medwaves Corporation. G. Jindal: Grant funding from Stryker and Medtronic unrelated to this publication.

[a] Russell H. Morgan Department of Radiology and Radiological Science, Johns Hopkins University School of Medicine, 600 North Wolfe Street, Phipps B100, Baltimore, MD 21287, USA; [b] Division of Interventional Neuroradiology, Department of Radiology, University of Maryland Medical Center, 22 South Greene Street, Baltimore, MD 21201, USA

* Corresponding author.

E-mail address: amodirs1@jhmi.edu

Neuroimag Clin N Am 29 (2019) 461–480
https://doi.org/10.1016/j.nic.2019.08.001

Table 1
Cervical spine MR imaging protocols

Sequence	Localizer	FLAIR	T2	T2	GRE	T1	T1	STIR	Enhanced T1	Enhanced T1
Plane	3 plane	Sagittal	Sagittal	Axial	Axial	Sagittal	Axial	Sagittal	Sagittal	Axial
Coil type	Neck	Neck	Neck	Neck	Neck	Neck	Neck	Neck	Neck	Neck
Thickness, mm	10	3	3	3	3	3	3	3	3	3
TR, ms	24	1700	3530	4210	32	653	649	4400	653	649
TE, ms	6	12	106	111	14	10	11	74	10	11
Flip angle	30	150	180	150	5	170	150	150	170	150
NEX	1	1	2	2	1	2	2	1	2	2
Matrix	128 × 256	250 × 384	269 × 384	240 × 320	216 × 320	269 × 384	205 × 256	192 × 256	269 × 384	205 × 256
FOV read, mm	300	260	240	200	200	240	240	240	240	240
FOV phase, mm	100	100	100	75	75	200	100	100	100	100
Comments								Trauma, Mets	If indicated	If indicated

Abbreviations: FLAIR, fluid-attenuated inversion-recovery imaging; FOV, field of view; GRE, gradient-recalled echo; Mets, metastases; NEX, number of excitations; STIR, short tau inversion recovery; TE, echo time; TR, repetition time.

Table 2
Thoracic spine MR imaging protocols

Sequence	Localizer	T1	T2	T2	STIR	Enhanced T1	Enhanced T1
Plane	3 plane	Sagittal	Sagittal	Axial	Sagittal	Sagittal	Axial
Coil type	Spine	Spine	Spine	Spine	Spine	Spine	Spine
Thickness, mm	10	4	4	4	4	4	4
TR, ms	20	641	3000	7360	3220	670	579
TE, ms	6	17	100	106	74	14	13
Flip angle	30	180	150	150	180	150	130
NEX	1	1	2	1	2	2	2
Matrix	128 × 256	256 × 256	307 × 384	192 × 256	256 × 256	269 × 384	230 × 256
FOV read, mm	380	300	320	200	320	320	200
FOV phase, mm	100	100	100	100	100	100	100
Comments					Trauma, Mets	If indicated	If indicated

Abbreviations: FOV, field of view; Mets, metastases; STIR, short tau inversion recovery; TE, echo time; TR, repetition time.

imaging of the spine. Axial gradient-echo images through the cervical spine are typically 2 mm thick.[2]

To depict the fine anatomic detail in the spine, high spatial resolution is a priority because of the small size of the cervical spine relative to the human body and because of the relatively superficial position of the spine within the human body. The use of surface coils, typically phased array receiver coils, helps to maximize signal-to-noise ratio and spatial resolution. Increasing phase-encoding steps results in a larger matrix and higher spatial resolution as a result, but also leads to increased imaging acquisition time, which increases the possibility of motion-related image degradation. Among the other factors affecting spinal imaging are matrix size, field of view, gradient moment nulling motion compensation, pulse triggering and gating, bandwidth, and phase-encoding axis.[3]

The pulse sequences used are determined by the clinical indications for the examination based

Table 3
Lumbar spine MR imaging protocols

Sequence	Localizer	T1 FLAIR	T2	T2	T1	STIR	Enhanced T1	Enhanced T1
Plane	3 plane	Sagittal	Sagittal	Axial	Axial	Sagittal	Sagittal	Axial
Coil type	Spine	Spine	Spine	Spine	Spine	Spine	Spine	Spine
Thickness, mm	10	4	4	4	4	4	4	4
TR, ms	3.27	1600	3150	4250	500	4560	657	539
TE, ms	1.64	12	95	106	14	79	12	14
Flip angle	55	150	180	150	90	180	90	90
NEX	2	1	2	1	1	2	2	1
Matrix	115 × 256	256 × 256	256 × 256	218 × 256	205 × 256	192 × 256	192 × 256	192 × 256
FOV read, mm	450	280	280	200	200	280	280	200
FOV phase, mm	100	100	100	100	100	100	75	100
Comments						Trauma, Mets	If indicated	If indicated

Abbreviations: FLAIR, fluid-attenuated inversion-recovery imaging; FOV, field of view; Mets, metastases; STIR, short tau inversion recovery; TE, echo time; TR, repetition time.

on the following major categories: degenerative disease including radicular symptomatology, trauma, cord compression/bony metastases, and infection.[4] Spin-echo and fast spin-echo sequences are the most common sequences used in spinal MR imaging. Short tau inversion recovery (STIR) imaging is useful to assess the bone marrow[5] and also in cases of infectious,[6] inflammatory,[7] and neoplastic[8] lesions. STIR imaging is also useful in the workup of trauma, to assess for ligamentous injury[9] and changes because of hemorrhage and/or edema. Contrast-enhanced imaging should be used, unless contraindicated, for indications including evaluation of the postoperative spine, suspected infection, or intradural or nontraumatic cord lesions.[10] Abnormalities within the epidural space identified during unenhanced evaluation for metastases and/or cord compression can be better delineated using contrast-enhanced images.[10]

Gradient-recalled echo (GRE), or gradient-echo, sequences allow for delineation of bone and disc margins, provide excellent contrast between the spinal cord and surrounding subarachnoid space, and allow clear visualization of the neural foramina and exiting nerve roots. Gradient-echo axial images are used in the cervical and thoracic spine to detect spinal canal and foraminal stenoses,[11] and serve as an important complement to long repetition time spin-echo imaging, given the faster acquisition time of GRE. As a result, GRE images are less susceptible to patient motion artifact. Although signal-to-noise ratio is increased with GRE, fat is of low signal intensity on GRE sequences compared with T1-weighted spin-echo imaging; as a result, morphologic detail defined by fat is not as well demonstrated on GRE images as on spin-echo images.[12]

Proton density images can be obtained simultaneously (repetition time [TR] 2000–3000 ms or greater, echo time [TE] 20–90 ms) when obtaining T1-weighted images and can also be derived from an earlier (first) echo while generating T2-weighted images. Proton density images of the spine are not routinely obtained but can provide valuable information concerning normal and pathologic spinal morphology.[5]

NORMAL SPINAL ANATOMY BASICS

The cervical spine comprises the first 7 superior vertebrae of the spinal column. The first and second segments of the cervical spine are unique. The other cervical vertebrae are similar in size and configuration. The first segment, C1, also known as the atlas, is ring shaped and consists of anterior and posterior arches and lateral articular masses. It lacks a central vertebral body. The second segment, C2, also known as the axis, is also ring shaped and has a superiorly oriented odontoid process, also known as the dens, which lies posterior to the anterior arch of C1. The normal distance between the dens and anterior arch of C1 is approximately 3 mm in adults and 4 mm in children.[13] There are prominent tubercles along the medial aspects of the lateral masses of C1 from which extend the transverse portion of the cruciate/cruciform ligament, that is, the transverse ligament, which confines the odontoid process of C2 posteriorly and delineates the anterior and posterior compartments. This relationship allows free rotation of C1 on C2 and provides for stability during upper cervical spinal flexion, extension, and lateral bending. The transverse ligament is covered posteriorly by the tectorial membrane. The alar ligaments are paired wing-like structures connecting the lateral aspects of the odontoid process with the occipital condyles. The thin apical ligament of the odontoid process directly anchors the tip of the odontoid process to the clivus in the anterior aspect of the foramen magnum. The tip of the odontoid process is anterior to the lower medulla. A line of low T1-weighted signal intensity seen through the base of the dens, with a correlative area of sclerosis on CT, represents the subdental synchondrosis, present in many healthy individuals; it may be distinguished from a fracture because the synchondrosis does not extend to the adjacent cortical bone (**Figs. 1** and **2**).

Unique to the cervical spine, the bilateral uncovertebral joints, also referred to as Luschka joints, are formed by articulation of the uncinate process of the inferior vertebral body with the uncus of the superior vertebral body (see **Fig. 2**; **Figs. 3** and **4**). The uncus is a cup-shaped groove on the posterior/inferior aspect of each cervical vertebral body (except C1), whereas the uncinate processes are located bilaterally on the posterosuperior aspects of the cervical vertebral bodies (except for C1 and C2). The cervical vertebrae also form transverse foramina bilaterally through which the vertebral arteries pass. Although the C7 vertebral body forms transverse foramina, the vertebral arteries usually enter the foramina at C6. The vertebral arteries are circular low signal structures owing to the flow-void phenomenon (see **Fig. 3**C). The spinous processes of the cervical spine are short and have bifid tips. Compared with the lumbar discs, the discs of the cervical and thoracic spine are much thinner and the outermost portion of the anulus is not as thick. The

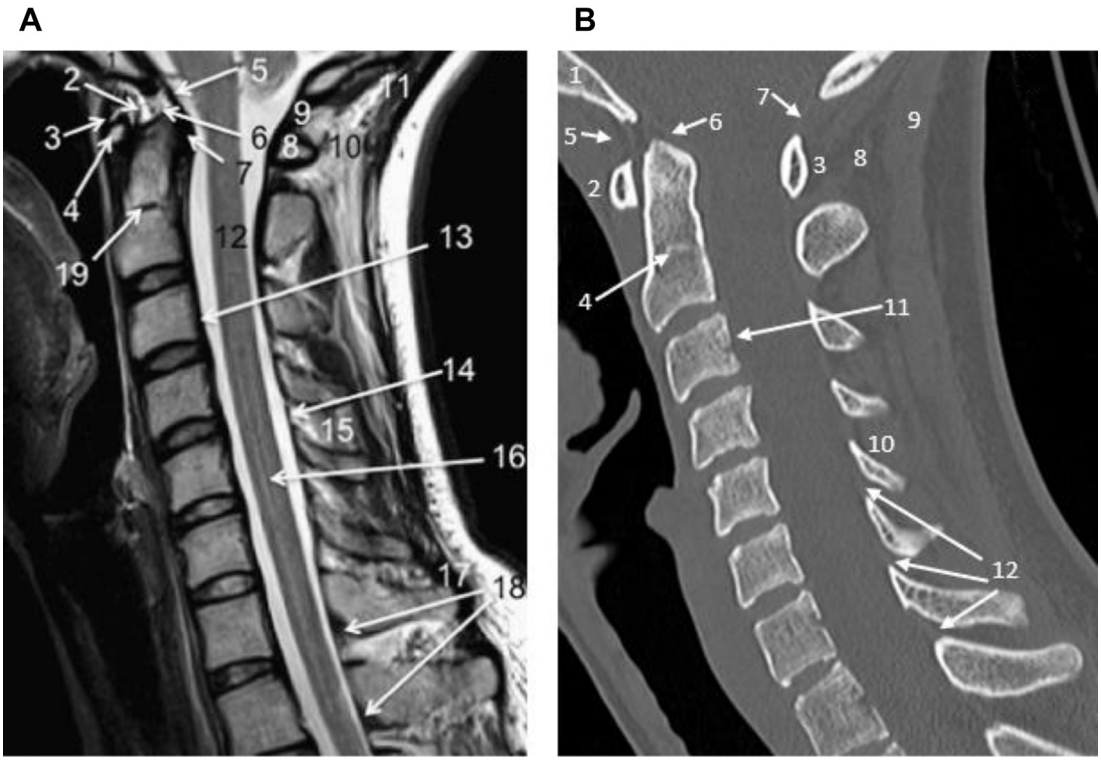

Fig. 1. (*A*) Sagittal T2-weighted image, cervical spine. 1, Clivus; 2, atlanto-occipital ligament; 3, anterior longitudinal ligament; 4, anterior arch C1; 5, superior fascicle of cruciform ligament/tectorial membrane; 6, apical ligament; 7, transverse ligament (of cruciform ligament); 8, posterior arch C1; 9, posterior occipital-atlantal membrane; 10, nuchal ligament; 11, semispinalis capitis muscle; 12, cervical spinal cord; 13, posterior longitudinal ligament/anterior thecal sac dura; 14, posterior dural sac; 15, interspinous ligament; 16, gray matter along central canal; 17, supraspinous ligament; 18, ligamentum flavum; 19, dental synchondrosis (disc anlage). (*B*) Sagittal CT image, cervical spine. 1, Clivus; 2, anterior arch C1; 3, posterior arch C1; 4, dental synchondrosis (disc anlage); 5, anterior longitudinal ligament; 6, tectorial membrane; 7, posterior occipital-atlantal membrane; 8, nuchal ligament; 9, semispinalis capitis muscle; 10, interspinous ligament; 11, posterior longitudinal ligament; 12, ligamentum flavum.

cervical spine is depicted in images in **Figs. 1–4**, **Figs. 5** and **6**.

Given the anterolateral-directed obliquity of the cervical neural foramina, oblique sagittal views are required to view cross-sectional sagittal anatomy of the neural foramina of the cervical spine.[14,15] In MR imaging, these images are obtained by using an axial image to first assess optimal angulation of the oblique sagittal plane through the foramina. Similar reconstructions can be performed with CT at the scanner based on the raw data. Alternatively, given the relatively routine availability of thin-section reconstructions, reformations in any plane, including the oblique sagittal plane through the foramina, can now be performed at the reading station on the picture archiving and communication system.

Throughout the spine, the intervertebral canals, or neural foramina, contain the nerve root and its sleeve, the dorsal root ganglion, fat, and blood vessels. The neural foramina are bounded anteriorly by the vertebral bodies and disc, superiorly and inferiorly by the pedicles, and posteriorly by the facet joints, which are covered by the ligamentum flavum (see **Fig. 3**).[16] The segmental osseous structures of the spine include the vertebral bodies and their appendages, including the pedicles, the articular pillars, laminae, and transverse and spinous processes. The major ligaments of the spine are the anterior longitudinal ligament, posterior longitudinal ligament, and ligamentum flavum (**Fig. 7**).[16] The spinal canal contains the thecal sac enclosed by the dura mater and surrounded by the epidural space, which contains epidural fat and a large venous plexus. Within the thecal sac are the spinal cord, conus medullaris, and cauda equina, surrounded by freely flowing CSF within the subarachnoid space. The conus medullaris normally terminates near the L1 vertebral level.[16] In the

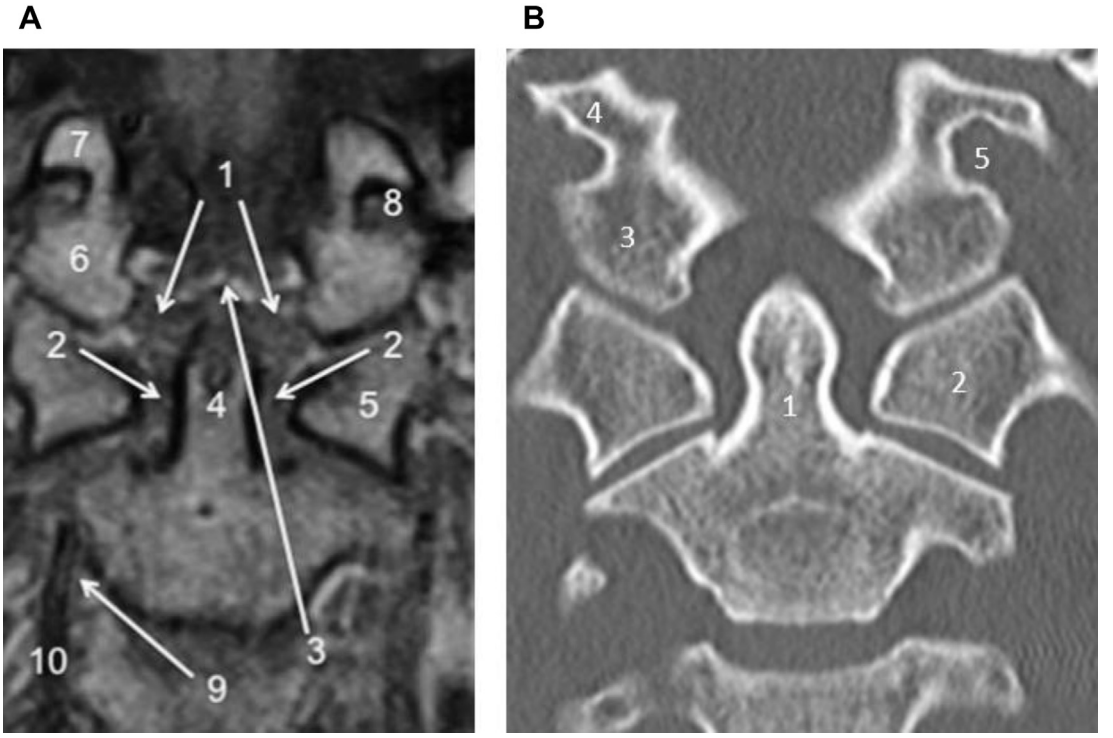

Fig. 2. (*A*) Coronal T1-weighted image, craniocervical junction. 1, Alar ligament; 2, transverse ligament (of cruciform ligament); 3, apical ligament; 4, dens; 5, lateral mass C1; 6, occipital condyle; 7, jugular tubercle of occipital bone; 8, hypoglossal canal; 9, uncinate process C3; 10, vertebral artery. (*B*) Coronal CT image, craniocervical junction. 1, Dens; 2, lateral mass C1; 3, occipital condyle; 4, jugular tubercle of occipital bone; 5, hypoglossal canal.

supine position, the nerve roots of the cauda equina in the lumbar spine are clustered in the dependent/posterior aspect of the spinal canal (**Figs. 8** and **9**).

The posterior border of nearly all of the vertebral bodies is flat or slightly concave when viewed in axial section, and the discs do not normally extend beyond the margins of the adjacent

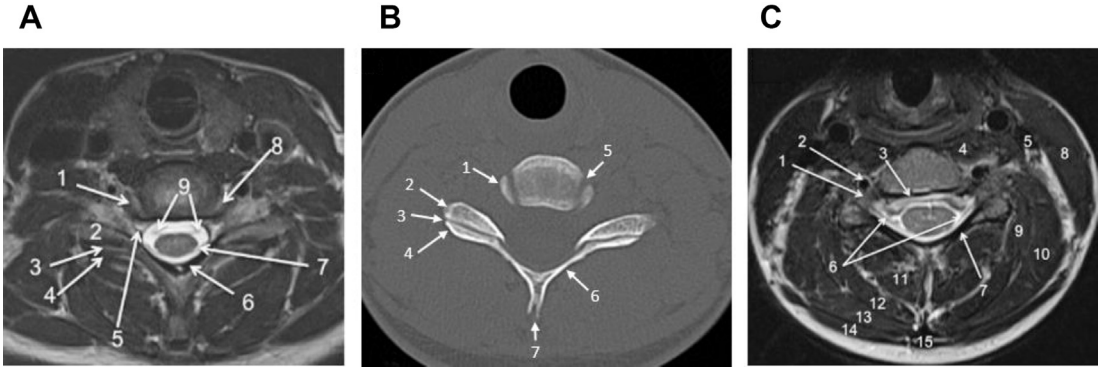

Fig. 3. (*A*) Axial T2-weighted image, lower cervical spine. 1, Uncinate process C7; 2, superior articular process C7; 3, apophyseal (facet) joint; 4, inferior articular process C6; 5, foraminal vein; 6, ligamentum flavum/cortex of lamina; 7, dorsal rootlet C7; 8, uncovertebral joint; 9, ventral rootlets C7. (*B*) Axial CT image, lower cervical spine. 1, Uncinate process C7; 2, superior articular process C7; 3, apophyseal (facet) joint; 4, inferior articular process C6; 5, uncovertebral joint; 6, lamina C6; 7, spinous process C6. (*C*) Axial T2-weighted image, mid-cervical spine. 1, Dorsal root ganglion; 2, vertebral artery; 3, posterior longitudinal ligament/anterior thecal sac dura; 4, longus colli muscle; 5, internal jugular vein; 6, dorsal rootlets; 7, lamina; 8, sternocleidomastoid muscle; 9, longissimus capitis muscle; 10, levator scapulae muscle; 11, semispinalis colli muscle; 12, semispinalis capitis muscle; 13, splenius capitis muscle; 14, trapezius muscle; 15, nuchal ligament.

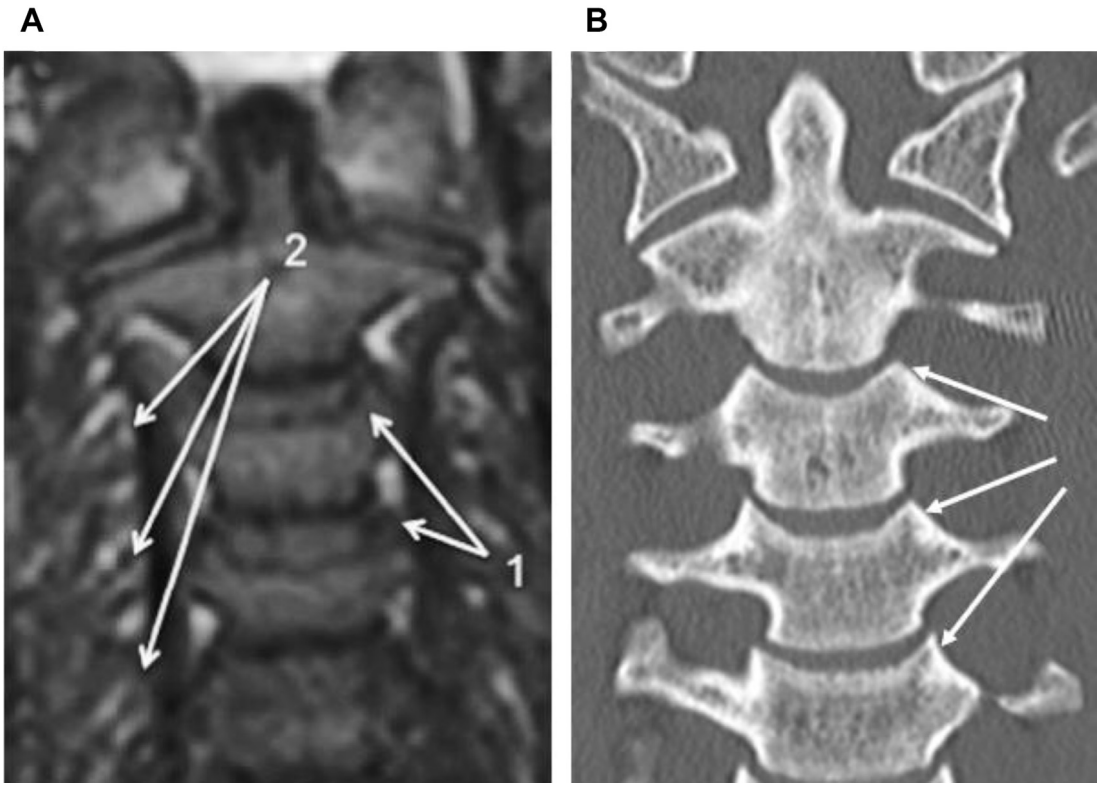

Fig. 4. (*A*) Coronal T1-weighted image, cervical spine. 1, Uncinate processes; 2, segmental spinal veins and nerve roots. (*B*) Coronal CT image, cervical spine. Arrows point to uncinate processes.

vertebral bodies.[16] However, with exaggerated extension, 1- to 2-mm budging may occur in some histologically normal discs.[17–19] The posterior margins of the discs tend to be slightly concave in the upper lumbar spine, straight at the L4/5 level, and slightly convex at the lumbosacral spinal junction. This appearance should not be confused with pathologic bulging. The axial appearance of the L5 vertebral body is biconcave, and iliolumbar ligaments emanate laterally from L5, characteristics that allow distinction of this vertebral segment from others when viewed in the axial plane (see **Fig. 9**). The spinal canal is round in the upper lumbar region and transitions to a triangular configuration in the lower lumbar region. Posterior epidural fat is consistently present in the posterior part of the spinal canal, whereas the anterior epidural fat is most prominent in the L5-S1 region (see **Fig. 8**).[16]

The bony canals of the neural foramina are normally well seen en face in the lumbar region using standard sagittal images (**Fig. 10**), because the orientation of the neural foramina in the lumbar spine is nearly directly lateral as opposed to the anterolateral angle of the neural foramina of the cervical spine. This is distinct from the anterior obliquity required to optimally visualize the neural foramina of the cervical spine in the sagittal plane.

NORMAL SPINAL ANATOMY, T1-WEIGHTED MR IMAGING

T1-weighted images (TR 300–500 ms, TE 20–30 ms) in the sagittal plane are obtained as the preliminary survey pulse sequence for analyzing the cervical, thoracic, and lumbar spine. Sagittal and axial T1-weighed sequences provide the anatomic detail with which to begin a survey of the spine.

On T1-weighted images, high signal intensity is demonstrated in mature bone marrow and the epidural fat. The normal bone marrow signal is usually homogeneous, but may be heterogeneous and normally changes with aging.[20] The basivertebral venous channel is seen on the midline sagittal images as a high signal within the posterior aspect of the vertebral body owing to fat surrounding the vein with correlative area of

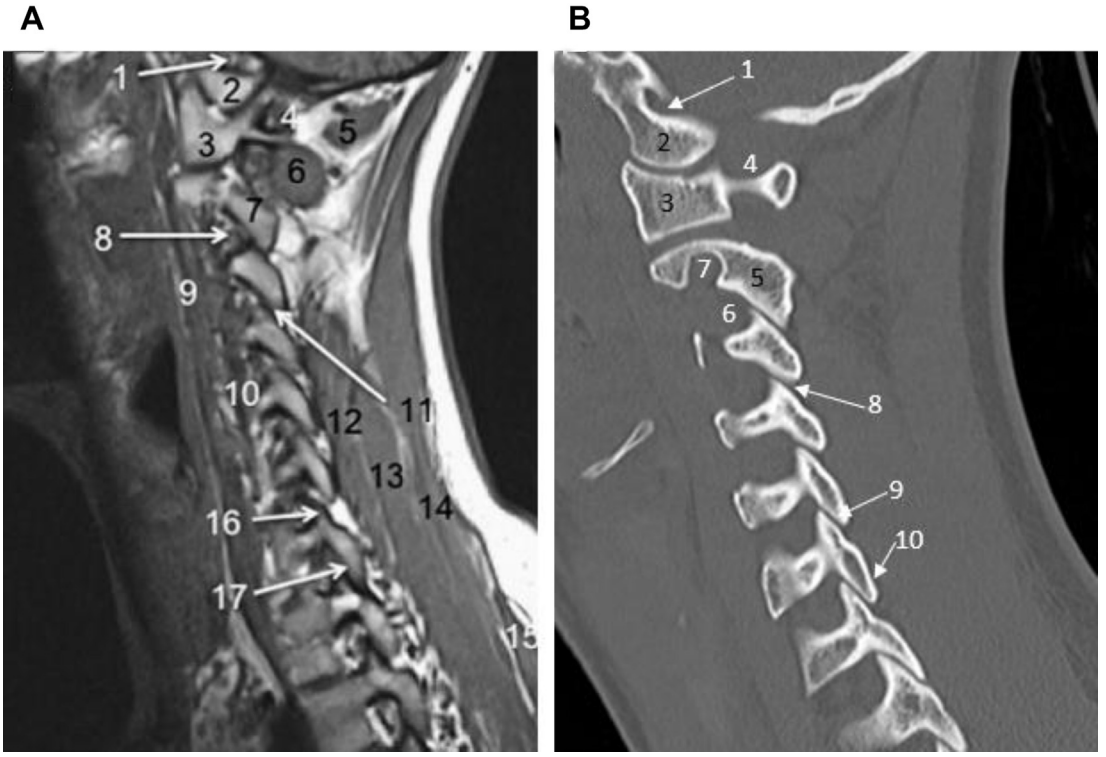

Fig. 5. (*A*) Parasagittal T1-weighted image, cervical spine. 1, Hypoglossal canal; 2, occipital condyle; 3, lateral mass C1; 4, vertebral artery; 5, rectus capitis posterior major muscle; 6, obliquus capitis inferior muscle; 7, articular pillar C2; 8, C3 dorsal root ganglion; 9, longus coli (cervicis) muscle; 10, vertebral artery; 11, apophyseal (facet) joint C3-4; 12, multifidis muscle; 13, semispinalis cervicis muscle; 14, splenius capitis muscle; 15, trapezius muscle; 16, superior articular process; 17, inferior articular process. (*B*) Parasagittal CT image, cervical spine. 1, Hypoglossal canal; 2, occipital condyle; 3, lateral mass C1; 4, groove for vertebral artery C1; 5, articular pillar C2; 6, C3 dorsal root ganglion location; 7, foramen transversarium C2 (contains vertebral artery); 8, apophyseal (facet) joint C3-C4; 9, superior articular process; 10, inferior articular process.

radiolucency on CT (see **Fig. 8**).[10] Peripherally, bone marrow is surrounded by low signal, proton-poor cortical bone, making it indistinguishable from the adjacent low T1-weighted signal intensity of the annulus fibrosus, spinal ligaments, and dura (see **Fig. 6**).[21] The relatively poor distinction between these structures on spin-echo imaging of the cervical and thoracic spine is attributable to little anterior epidural fat compared with that in the lumbar spine (see **Figs. 6** and **8**). Spin-echo imaging often also poorly differentiates cortical osteophytes from disc material. The anterior and posterior longitudinal ligaments adhere to the fibers of the annulus and appear on midsagittal images as an uninterrupted band of very low signal intensity on all pulse sequences (see **Figs. 8** and **10**).[21]

The intervertebral discs demonstrate slightly less signal than the adjacent vertebral bodies and differentiation of the centrally located nucleus pulposis and peripheral annulus fibrosis of the discs cannot be made precisely on T1-weighted images (see **Figs. 8** and **10**).

CSF demonstrates low signal on T1-weighted images and provides contrast with the adjacent, relatively higher signal intensity spinal cord and nerve roots within the spinal canal. The periphery of the spinal canal is lined by high signal-intensity epidural fat (see **Fig. 9**). The nerve roots and dorsal ganglia occupy the upper portion of the neural foramina, also referred to as the subpedicular notch (see **Fig. 10**), and appear as rounded low signal structures surrounded by high signal fat in the neural foramina. The nerve roots can be followed through the neural foramina on sagittal images. Epidural veins appear as signal voids anterosuperior to the nerves. It is important to distinguish the ventral internal longitudinal vein from the adjacent nerve and ganglion (see **Figs. 6**, **9**, and **10**). Each intervertebral canal can be divided arbitrarily into superior and inferior portions. The superior portion of the canal contains

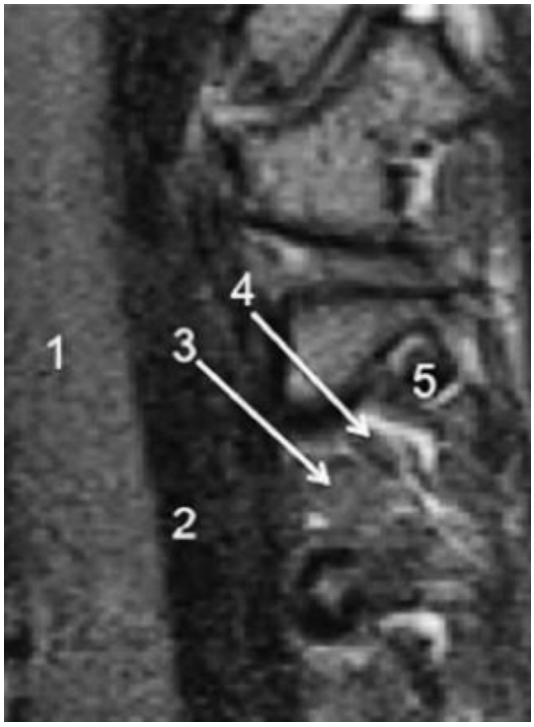

Fig. 6. Coronal oblique T1-weighted image, cervical spine. 1, Cervical spinal cord; 2, subarachnoid space; 3, dorsal root ganglion; 4, superior foraminal vein; 5, vertebral artery.

the dorsal root ganglion, veins, and epidural fat. The inferior portion contains the nerves, which lie below the disc level close to the superior articular process of the facet joint.[2]

The facet joints appear as linear structures with intermediate signal owing to the presence of intra-articular hyaline cartilage and synovial fluid (see Fig. 9).[22] The facet joint is formed by the concave surface of the superior articular process and the convex surface of the inferior articular process (see Fig. 10). The superior facet is located anterolaterally and faces posteromedially. The inferior facet is located posteromedially and faces anterolaterally. This differs in the cervical spine, where the superior and inferior articular processes are fused on either or both sides to form articular pillars, columns of bone that project laterally from the junction of the pedicle and lamina. The bony processes of the spine are better delineated on CT as compared with MR imaging. The ligamentum flava, which bilaterally cover the inner surface of the lamina and the anterior aspects of the facet joints, are intermediate in signal intensity and are distinguishable from the adjacent high signal central epidural fat and adjacent peripheral low signal lamina (see Fig. 9; Fig. 11).

NORMAL SPINAL ANATOMY, T2-WEIGHTED MR IMAGING

The parameters of T2-weighted imaging include a TR of 2000 to 3000 ms and a TE of 60 to 120 ms; the acquisition time is 2 to 3 times longer than that of T1-weighted imaging, rendering T2-weighted imaging more susceptible to motion artifact and greater noise.

In general, T2-weighted images reveal greater contrast differentiation among structures in

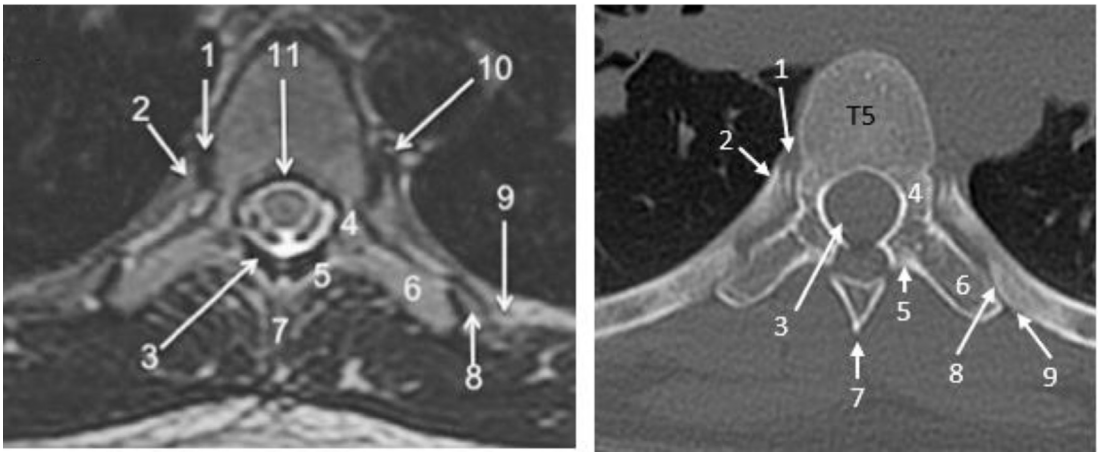

Fig. 7. (*A*) Axial T2-weighted image, thoracic spine. 1, Costovertebral joint; 2, head of rib; 3, ligamentum flavum; 4, pedicle; 5, lamina; 6, transverse process; 7, spinous process; 8, costotransverse joint; 9, tubercle of rib; 10, hemiazygous vein; 11, posterior longitudinal ligament. (*B*) Axial CT image, thoracic spine. 1, Costovertebral joint; 2, head of rib; 3, ligamentum flavum; 4, pedicle T5; 5, lamina T5; 6, transverse process T5; 7, spinous process T4; 8, costotransverse joint; 9, tubercle of rib.

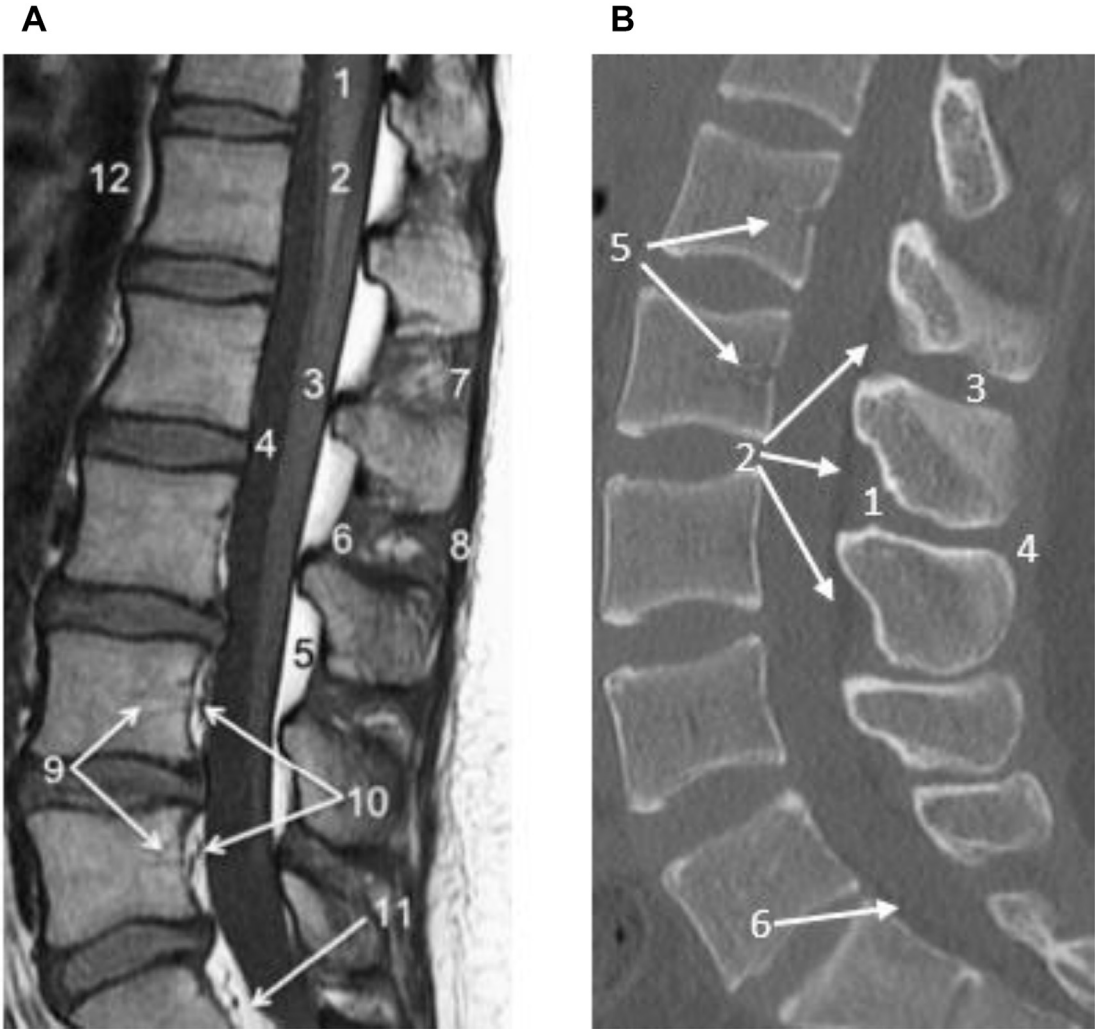

Fig. 8. (*A*) Sagittal T1-weighted image, lumbar spine. 1, Spinal cord; 2, conus medullaris; 3, cauda equina; 4, subarachnoid space; 5, posterior epidural fat; 6, ligamentum flavum; 7, interspinous ligament; 8, supraspinous ligament; 9, basivertebral venous plexus; 10, epidural venous plexus; 11, anterior epidural fat; 12, aorta. (*B*) Sagittal CT image, lumbar spine. 1, Ligamentum flavum; 2, posterior epidural fat; 3, interspinous ligament; 4, supraspinous ligament; 5, basivertebral venous plexus; 6, anterior epidural fat.

comparison with T1-weighted images. With T2 weighting, the proton-poor cortical bone demonstrates low signal intensity and the bone marrow remains fairly high in signal intensity because of its fat content. The basivertebral veins may be of even higher signal intensity because of flow phenomena and should not be mistaken for a fracture (**Fig. 12**). The channel of the basivertebral vein is usually of intermediate signal on the T2-weighted image. The normally hydrated nucleus pulposus composed of water and proteoglycans shows high T2-weighted signal centrally, with lower signal from the less-hydrated annulus fibrosis (see **Fig. 12**). The annulus fibrosis is composed of fibrocartilage centrally, whereas the outer fibers are made up of concentrically oriented collagen fibers. The annulus is anchored to the adjacent vertebral bodies by Sharpey fibers, which are normally not visible by MR imaging.

CSF demonstrates high signal intensity because of its long T2-weighted relaxation time, which allows sensitive identification of surrounding intraspinal structures such as the spinal cord and nerve roots that are intermediate in signal intensity (see **Fig. 12**; **Figs. 13–15**). When the patient is supine, as in most cases of spinal imaging, the mid-thoracic spinal cord is positioned within the central/anterior aspect of the

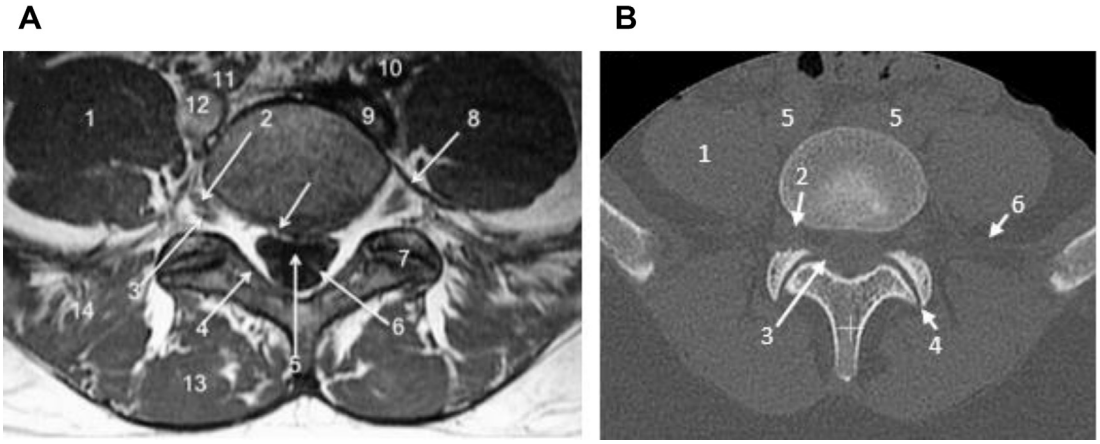

Fig. 9. (*A*) Axial T1-weighted image, lumbar spine at L5-S1. 1, Psoas muscle; 2, L5 nerve root, ventral ramus; 3, L5 nerve root, dorsal ramus; 4, ligamentum flavum; 5, subarachnoid space; 6, nerve roots of cauda equina; 7, facet joint; 8, iliolumbar ligament (signifies L5 vertebral level); 9, left external iliac vein; 10, left external iliac artery; 11, right external iliac artery; 12, right external iliac vein; 13, transversospinalis (multifidis) muscle; 14, erector spinae muscle group. (*B*) Axial CT image, lumbar spine at L5-S1. 1, Psoas muscle; 2, L5 nerve root; 3, ligamentum flavum; 4, facet joint; 5, iliac vasculature; 6, iliolumbar ligament.

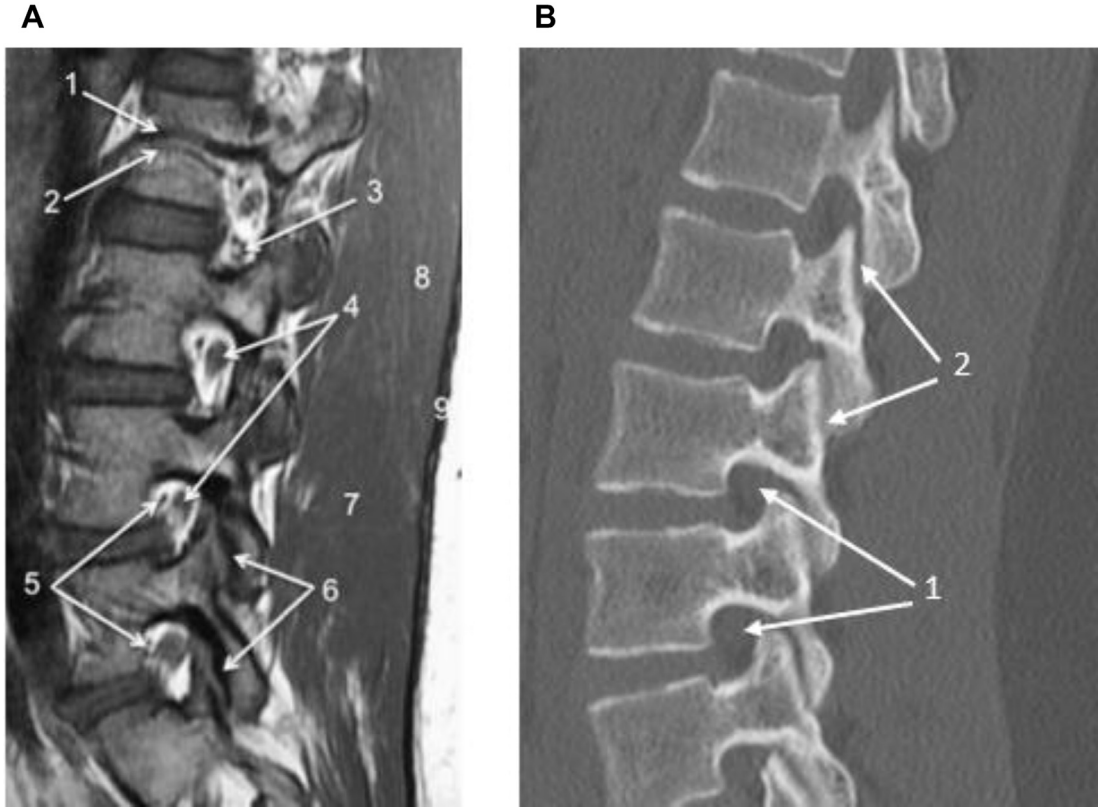

Fig. 10. (*A*) Parasagittal T1-weighted image, lumbar spine. 1, Lumbar vein; 2, lumbar artery; 3, inferior foraminal veins; 4, dorsal root ganglia; 5, superior foraminal veins; 6, facet joints; 7, transversospinalis (multifidis) muscle; 8, erector spinae muscle group; 9, thoracolumbar fascia, posterior layer. (*B*) Parasagittal CT image, lumbar spine. 1, Dorsal root ganglia/lumbar nerve roots; 2, facet joints.

Fig. 11. (*A*) Sagittal T1-weighted image, thoracic spine. 1, Thoracic spinal cord; 2, subarachnoid space; 3, posterior epidural fat; 4, ligamentum flavum; 5, transversospinalis (multifidus) muscle; 6, spinous process; 7, epidural vein; 8, supraspinous ligament. (*B*) Correlative Sagittal CT image, thoracic spine. The posterior epidural fat and the ligamentum flavi can be seen.

spinal canal owing to the normally mild thoracic kyphosis (see **Fig. 12**). CSF often has patchy areas of low signal because of turbulence of flow and/or other flow artifacts related to pulsation effects; these can be particularly troublesome in images with longer echo delays and in those acquired using high magnetic field strength systems (see **Fig. 14**).

T2* images intensify structures with long T2 relaxation times, such as CSF, the nucleus pulposis, and facet joint cartilage. On T2* images, the high signal intensity of the venous plexus posterior to the vertebral body separates the posterior longitudinal ligament and cortical bone of the vertebral body. T2* imaging also allows differentiation of the gray and white matter of the spinal cord. Gray matter appears as a butterfly-shaped region of high signal intensity centrally within the spinal cord when using this technique.[23]

NORMAL SPINAL BONE MARROW MR IMAGING

The axial skeleton contains red marrow, a major site of hematopoiesis throughout life. There is normally a gradual conversion of red marrow to fatty marrow in the appendicular skeleton, which

Fig. 12. Sagittal T2-weighted image, thoracic spine. 1, Thoracic spinal cord; 2, subarachnoid space; 3, ligamentum flavum; 4, transversospinalis (multifidus) muscle; 5, spinous process; 6, supraspinous ligament; 7, basivertebral vein; 8, conus medullaris; 9, cauda equina.

is completed by approximately 25 years of life. The red marrow in the vertebrae also normally undergoes conversion of fatty marrow, although more subtly than in the appendicular skeleton. The fat content of the vertebral body varies with age, degeneration of adjacent discs, therapy, such as radiation, and increased hematopoiesis in processes such as sickle cell disease or other diseases affecting the bone marrow.[20] In younger patients, high signal fatty marrow can be seen as linear areas adjacent to the

Fig. 13. Parasagittal T2-weighted image, thoracic spine. 1, Posterior thecal sac dura; 2, posterior epidural fat; 3, ligamentum flavum.

basivertebral vein. With advancing age, fatty marrow may appear band-like, triangular, or multifocal, and may take up relatively large areas of the vertebral body in patients older than 40 years.[20] There is significant variability in the marrow pattern among adults and even within an individual.[20,24]

Ricci and colleagues[25] identified several patterns of marrow distribution in the spine. In pattern 1, the vertebral body demonstrates uniformly low signal on T1-weighted images except for linear areas of high, fatty signal surrounding the basivertebral vein. In pattern 2, band-like and triangular areas of high signal are found near the end plates and corners of the vertebral body, possibly related to mechanical stress near the end plates. In pattern 3, there are diffusely distributed areas of high signal from fat measuring a few millimeters (pattern 3a) or relatively well-marginated areas on the range of 1 cm (pattern 3b).

In the cervical spine, pattern 1 is found predominantly in patients younger than 40 with patterns 2 and 3 in those who are older than 40 years. Patterns 2 and 3 generally develop earliest in the lumbar spine, followed by the thoracic spine, and lastly in the cervical spine.[25] Overall, there is continued gradual replacement of hematopoietic marrow with fatty marrow that continues until death. Healthy elderly individuals have marked high signal throughout the vertebral body, reflecting the predominance of fatty marrow. Large variations exist, however, secondary to differences among individuals and responses to mechanical stress.[25]

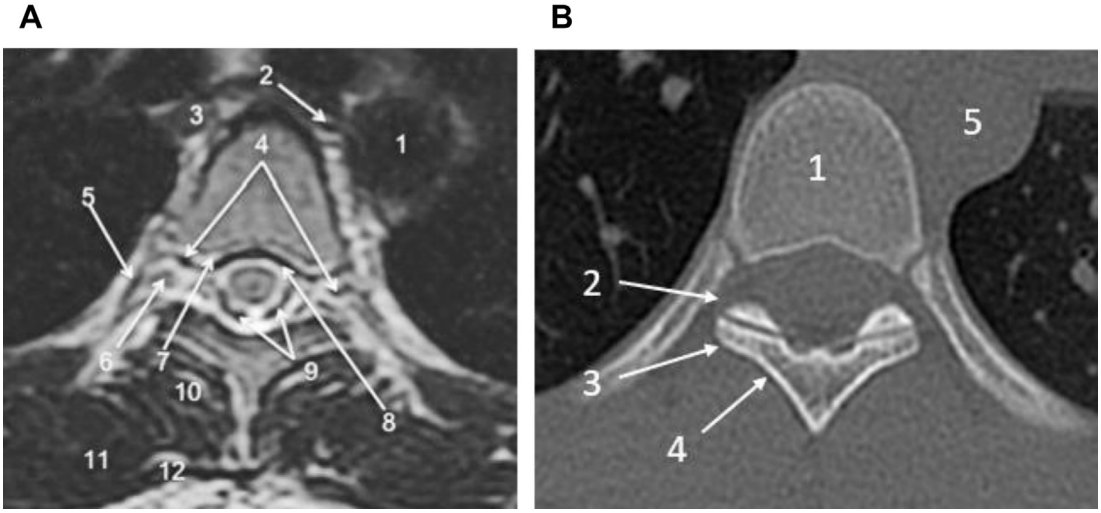

Fig. 14. (*A*) Axial T2-weighted image, thoracic spine. 1, Aorta; 2, hemiazygous vein; 3, azygous vein; 4, foraminal veins; 5, thoracic intercostal vein; 6, dorsal root ganglion; 7, basivertebral veins, slow flow; 8, posterior longitudinal ligament; 9, CSF flow artifacts; 10, transversospinalis (multifidis) muscle; 11, longissimus dorsi muscle; 12, trapezius muscle. (*B*) Axial CT image, thoracic spine. 1, T8 vertebral body; 2, T9 superior articular process; 3, T8 inferior articular process; 4, T8 right lamina; 5, aorta.

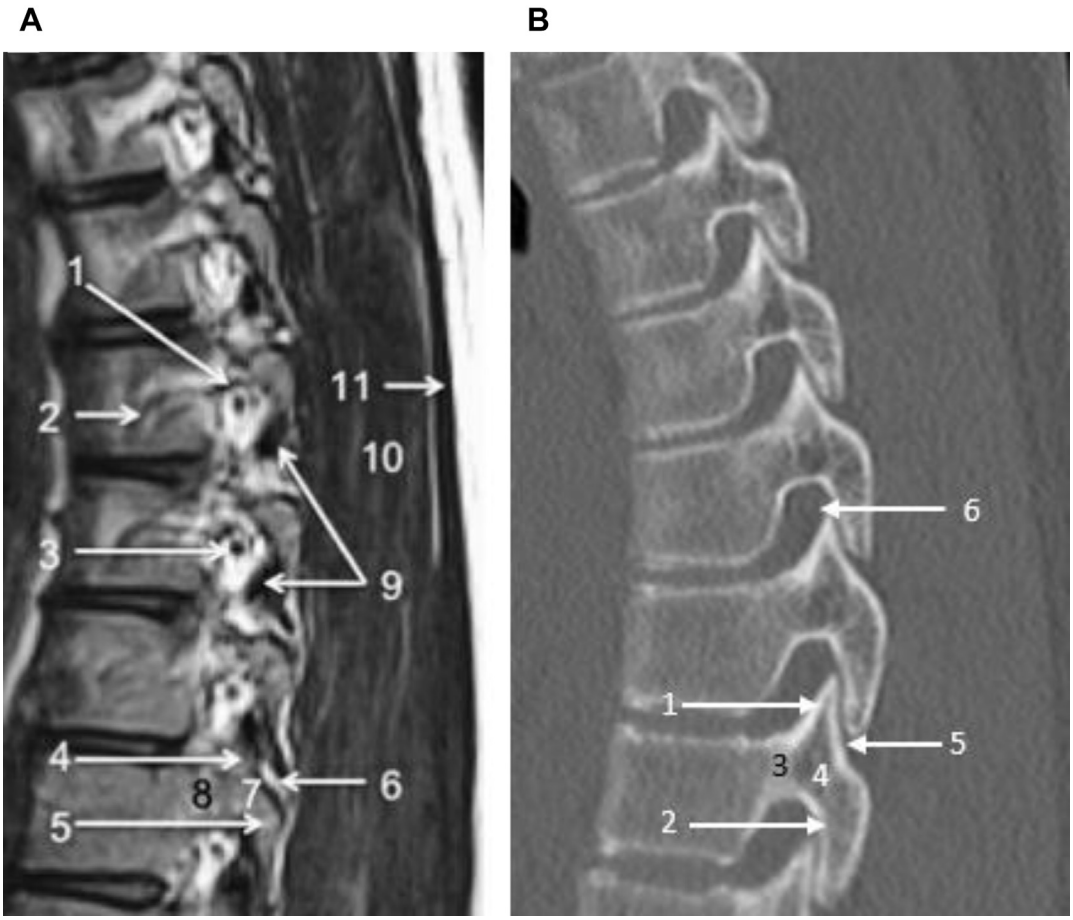

Fig. 15. (*A*) Parasagittal T2 weighted image, thoracic neural foramen. 1, Foraminal vein; 2, Thoracic paravertebral intercostal vein and artery; 3, Foraminal nerve root; 4, Superior articular process; 5, Inferior articular process; 6, Facet joint; 7, Pars interarticularis; 8, Pedicle; 9, Ligamentum flavum; 10, Erector spinae muscle group; 11, Trapezius muscle. (*B*) Parasagittal CT image, thoracic neural foramen. 1, Superior articular process; 2, Inferior articular process; 3, Pedicle; 4, Pars interarticularis; 5, Facet joint; 6, Neuroforamen with foraminal nerve root.

Chemical shift artifact, used extensively in imaging of the adrenal glands and the liver, can be used to assess the bone marrow of the spine in certain instances. In-phase/opposed-phase imaging assesses for the presence of fat and water in a voxel of tissue. The technique takes advantage of the fact that water and fat protons precess at different frequencies and without a refocusing pulse; when there are both fat and water protons in a given voxel, there will be some signal intensity loss on images that are obtained when the protons are in their opposed phase. The utility of chemical shift imaging lies in that cases of spinal neoplastic disease, normal fat-containing marrow is replaced with tumor, which can result in lack of signal suppression on the opposed-phase images. There have been a few reports that have described in-phase/opposed-phase imaging of the spinal bone marrow.[26–28]

MYELOGRAPHY

Myelography is a minimally invasive technique that allows better visualization of the intrathecal contents by administering a positive contrast agent. A lumbar puncture is performed and contrast is delivered percutaneously into the intrathecal space typically through a 22-gauge spinal needle. This technique allows evaluation of the spine in individuals who would otherwise benefit from an MR imaging but are unable to receive one because of some contraindication or the presence of hardware which would otherwise produce artifact and subsequently degrade the examination.

Before the current use of water-soluble nonionic contrast agents, agents such as air and lipiodol were used in conjunction with radiography to help image spinal tumors as early as the 1920s.[29] Lipiodol came with multiple complications including

chronic adhesive arachnoiditis.[30] In the 1940s, pantoopaque was used, which still gave rise to cases of arachnoiditis and other complications.[29] Use of plain radiographs for imaging was used until the 1970s when CT began to increase in usage.[29]

Common indications for the utilization of this technique would be in postsurgical patients, those with spinal stenosis and contraindication to MR imaging, radiation therapy treatment planning, and spinal CSF leak evaluation. The bony anatomy on imaging is the same as exemplified on normal CT. On fluoroscopy, after injection of subarachnoid contrast material, the contrast should spread out in the thecal space in a rostral-caudal manner, with positive outlining of the cauda equina nerve roots. On fluoroscopy, the bony anatomic landmarks and the positive contrast in the spine should appear as in Fig. 16. With subsequent performance of a CT myelogram, the intrathecal contents including the spinal cord and nerve roots can be well visualized (Fig. 17).

An advanced imaging technique used with myelography is dual energy CT with isolation of the CSF

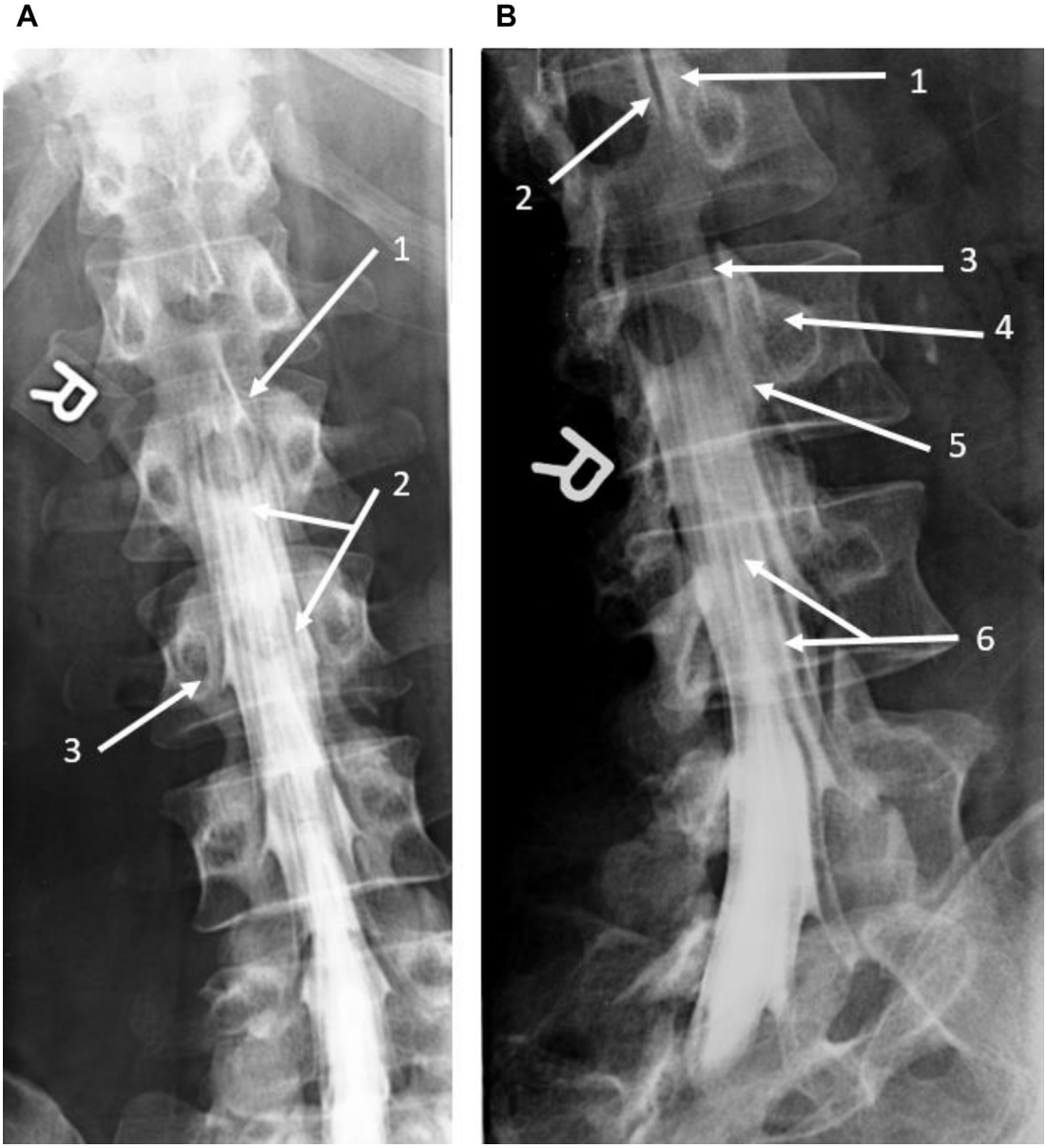

Fig. 16. (*A*) AP spot fluoroscopic image. 1, Spinous process; 2, cauda equina nerve roots outlined by contrast; 3, pedicle. (*B*) Oblique spot fluoroscopic image. 1, Inferior articular process; 2, superior articular process; 3, facet joint; 4, pedicle; 5, pars interarticularis; 6, contrast outlining cauda equina nerve roots.

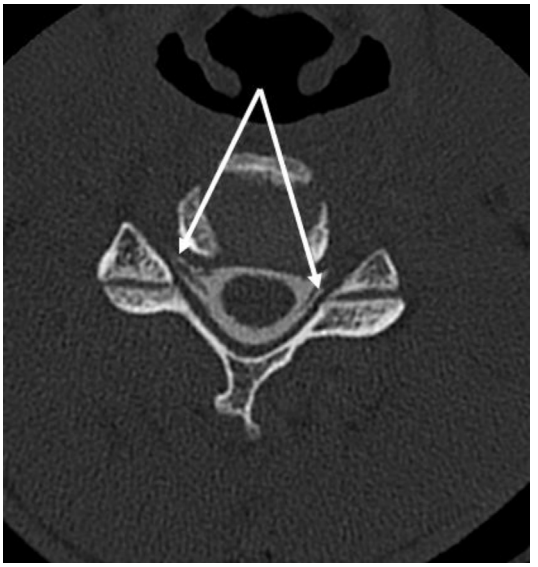

Fig. 17. Axial postcontrast cervical CT myelogram. Arrows point to the nerve roots outlined by intrathecal contrast.

column or using a bone subtracting algorithm to help better visualize the intrathecal space. These methods can be particularly useful in cases of subtle CSF leak or identifying focal areas of CSF diverticula. As is shown in **Fig. 18**, the intrathecal contrast column can be subtracted from the surrounding tissues. In **Fig. 19**, utilizing a CT algorithm to extract the bone is shown to be useful in focusing on the thecal sac and evaluating for areas of leak.

MR IMAGING FINDINGS OF VERTEBRAL HEMANGIOMAS

Hemangiomas, composed of angiomatoid fibroadipose tissue interspersed among tortuous thin-walled sinuses, are the most common benign tumors of the spine, seen in 10% or more of healthy adults.[31] They are most common in the thoracic spine followed by the lumbar spine, and are relatively rare in the cervical spine.[31] They tend to be well-circumscribed tumors within the vertebral bodies, demonstrating high signal intensity on both T1-weighted and T2-weighted images. T1 shortening is produced by the fatty component, whereas T2 prolongation is produced by the angiomatous component. The very low signal of the bony trabeculae, which can classically be seen on CT and result in the classic "polka dot" or "corduroy" appearance, is overshadowed on MR imaging by the signals from the internal elements described previously. Focal fatty infiltration, a common marrow variant, may be confused with hemangiomas on T1-weighted images; however, the expected corresponding decrease in signal intensity on T2-weighted images serves to distinguish focal fat from the normally high T2-weighted signal of hemangiomas.[32] Hemangiomas may sometimes have a paucity of fatty elements, which may render these lesions isointense or hypointense on T1-weighted images.[32]

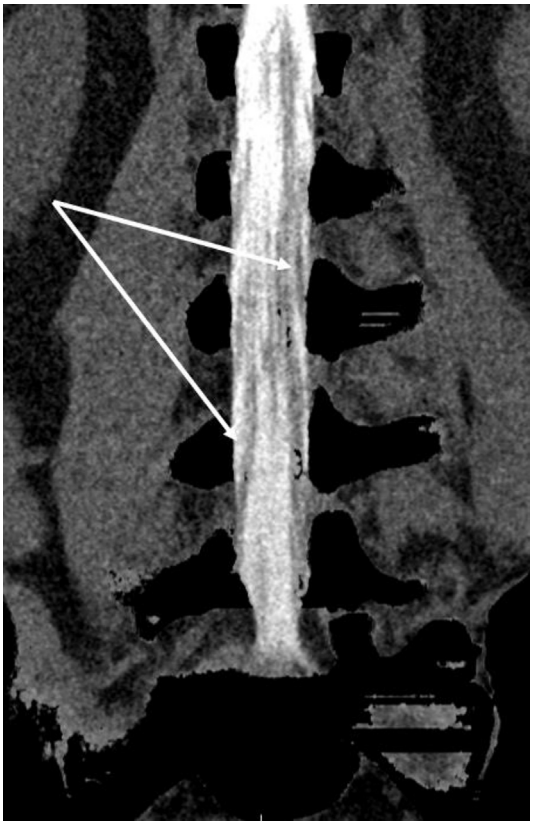

Fig. 18. Coronal dual energy CT myelogram with bone subtraction algorithm. Arrows point to the clearly outlined nerve roots of the cauda equina.

NORMAL MR IMAGING OF INTERVERTEBRAL DISCS

In the neonate, the nucleus pulposis is a highly gelatinous, translucent, relatively large, ovoid structure. The anulus fibrosus consists of dense fibers organized as concentric lamellae similar to tree rings. In the second decade of life, the outer portion of the disc is replaced by solid tissue and the anulus becomes more dense. In adults, the nucleus pulposis consists of amorphous fibrocartilage and the anulus becomes even more dense. The demarcation between the nucleus and anulus becomes less distinct with age. In adults, a transversely oriented band of low signal intensity in the

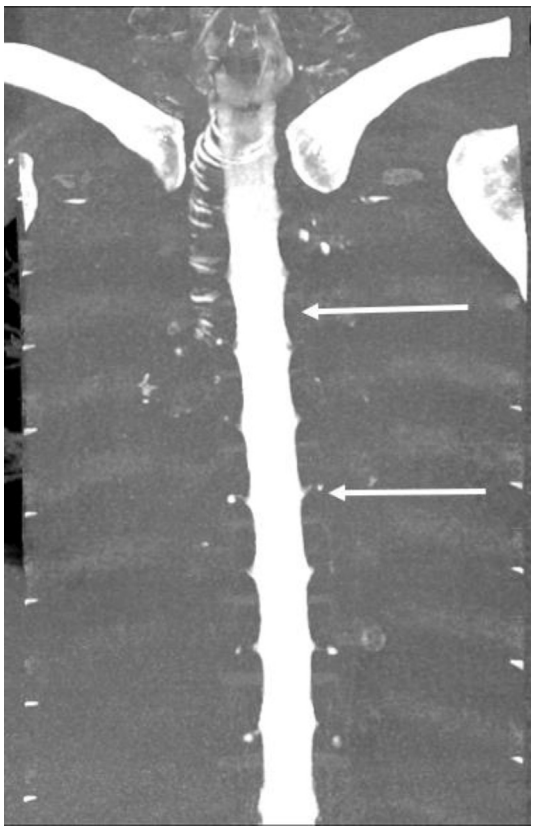

Fig. 19. Coronal dual energy subtracted thoracic myelogram. Arrow points to the intrathecal contrast column. Arrowhead highlights small outpouchings at the nerve roots.

midportion of the disc represents a fibrous plate visible on MR imaging. Concentric tears of the annulus are seen in normal discs, and transverse tears, although a manifestation of degenerative disease, are not infrequently seen in asymptomatic adults.[17,19]

Intervertebral herniation of disc material may remodel the vertebral end plate or may extend into the vertebral body. Such herniations are typically referred to as Schmorl nodes.[31] This type of herniation is presumed to have little clinical significance, and it has been observed as early as the second decade of life.

There are abnormalities and normal variants that may mimic the appearance of an extruded or sequestered disc on MR imaging. These include synovial cysts, dilated nerve root sleeves (arachnoid diverticulae), perineural cysts, conjoined nerve roots, nerve sheath tumors, and foreign material such as bullet fragments, metallic hardware, and cement from vertebroplasties. Dilated nerve root sleeves demonstrate signal characteristics identical to CSF, which should allow for differentiation of these from disc material.[4]

COMMON NORMAL SPINAL MR IMAGING ARTIFACTS

The most common source of artifact in MR imaging occurs secondary to patient motion. Whereas random movement leads to blurring, periodic motion, such as with CSF pulsation, cardiac motion, and respiratory motion, leads to ghosting artifacts in the form of image harmonics along the phase-encoding direction because phase information is acquired over an entire scan (minutes), whereas frequency information is acquired over a single frequency readout (milliseconds).[21]

CSF flow-related phenomena can be divided into time-of-flight (TOF) effects and turbulent flow, which produces dark signal. TOF effects are divided into TOF signal loss resulting in dark CSF signal and flow-related enhancement producing bright CSF signal. TOF loss typically occurs in spin-echo or fast spin-echo imaging when protons do not experience both the initial radiofrequency pulse and the subsequent radiofrequency refocusing pulse. TOF loss effects are more pronounced (darker signal) with faster proton velocity, thinner slices, longer TE, and an imaging plane perpendicular to flow. GRE techniques are less susceptible to TOF loss because of the short TE.

Typical locations for TOF losses include the lateral ventricles just superior to the foramen of Monro, the third ventricle, the fourth ventricle, and within the cervical and thoracic spinal canal. Given the positive relationship between CSF velocity and TOF losses, this effect is magnified in individuals with an underlying abnormally hyperdynamic state, such as hydrocephalus. In addition, laminar flow results in peripherally located protons moving at a slower velocity and leads to a reduction in TOF losses. Turbulent flow results in a broader spectrum of proton velocities and a wide range of flow directions that are not seen in typical laminar flow. This results in more rapid dephasing and signal loss termed "intravoxel dephasing." A commonly encountered CSF flow artifact is the signal void in the dorsal subarachnoid space on sagittal T2-weighted images of the thoracic spine owing to a combination of the respiratory-related and cardiac-related pulsatile CSF flow superimposed on cranially directed bulk CSF flow and turbulent flow from CSF moving from the ventral subarachnoid space to the dorsal subarachnoid space (see **Fig. 14**; **Fig. 20**).

Another common artifact that occurs normally on MR imaging relates to chemical shift and occurs because water and fat protons resonate at slightly different frequencies because of the

Fig. 20. Sagittal T2-weighted image demonstrating CSF pulsation artifact within the posterior aspect of the thecal sac (*asterisk*).

effects of their local magnetic environment. The most common type of chemical shift artifact occurs along the frequency-encoding axis and results in a spatial misregistration.[33] In the spine, this artifact is manifested as artifactual black lines along the frequency-encoding axis

Fig. 21. Artifact degraded sagittal T2-weighted image, thoracic spine. Truncation artifacts (*asterisk*). Truncation artifact simulating spinal cord syrinx (*solid white arrow*).

and are most evident in the sagittal T1-weighted images where they produce asymmetric thicknesses of the vertebral end plates. The hyaline cartilage end plate is usually difficult to visualize on MR imaging owing to overlap from chemical shift artifact.[34] Phase-encoding and frequency-encoding gradients may be reversed for imaging the spine in the sagittal plane to avoid chemical shift artifacts in the end plates and discs from the discovertebral interfaces.[34] Chemical shift is proportional to the magnetic field strength.

Truncation artifact, known as Gibb phenomenon, is seen as bands parallel to the spinal cord. This occurs at the interface of CSF and spinal cord because of high-contrast boundaries and is related to acquisition parameters, such as field of view and voxel size (**Fig. 21**).[35,36]

SUMMARY

Spinal MR imaging is an excellent tool for identifying details of spinal anatomy, including the intraspinal contents, neural foramina, joints, ligaments, intervertebral discs, and bone marrow. The cortical bony structures of the spine, as elsewhere in the body, are generally better imaged using CT. Conventional and CT myelography is an alternative to MR imaging in those with contraindications to MR imaging or in the evaluation of spinal CSF leaks. Motion-related and flow-related artifacts may occur during spinal MR imaging and should not be mistaken for a pathologic condition. As advancements continue to be made in both MR imaging hardware and software, spinal MR imaging can continue to expand its role in the delineation of normal and abnormal spinal anatomy.

REFERENCES

1. Brown BM, Schwartz HR, Frank E, et al. Preoperative evaluation of cervical radiculopathy and myelopathy by surface-coil MR imaging. AJNR Am J Neuroradiol 1988;9:859–66.
2. Norman D, Mills CM, Grant-Zawadzki M, et al. Magnetic resonance imaging of the spinal cord and canal: potentials and limitations. AJR Am J Roentgenol 1983;141:1147–52.
3. Chan WP, Lang P, Genant HK, et al. MRI of the musculoskeletal system. Philadelphia: W.B. Saunders Company; 1994.
4. Kaplan PA, Helms CA, Dussault R, et al. Musculoskeletal MRI. Philadelphia: W.B. Saunders Company; 2001.
5. Demaerel P, Sunaert S, Wilms G. Sequences and techniques in spinal MR imaging. JBR-BTR 2003; 86:221–2.
6. Dagirmanjian A, Schils J, McHenry MC. MR imaging of spinal infections. Magn Reson Imaging Clin N Am 1999;7:525–38.
7. Maksymowych WP, Crowther SM, Dhillon SS, et al. Systematic assessment of inflammation by magnetic resonance imaging in the posterio elements of the spine in ankylosing spondylitis. Arthritis Care Res 2010;62:4–10.
8. Myslivecek M, Nekula J, Bacovsky J, et al. Multiple myeloma: predictive value of tc-99m mibi scintigraphy and MRI in its diagnosis and therapy. Nucl Med Rev Cent East Eur 2008;11:12–6.
9. Williams RL, Hardman JA, Lyons K. MR imaging of suspected acute spinal instability. Injury 1998;29: 109–13.
10. Breger RK, Williams AL, Daniels DL, et al. Contrast enhancement in spinal MR imaging. AJNR Am J Neuroradiol 1989;10:633–7.
11. Hedberg MC, Drayer BP, Flom RA, et al. Gradient echo (GRASS) MR imaging in cervical radiculopathy. AJNR Am J Neuroradiol 1988;9:145–51.
12. Wang M, Dai Y, Han Y, et al. Susceptibility weighted imaging in detecting hemorrhage in acute cervical spinal cord injury. Magn Reson Imaging 2011;29: 365–73.
13. Parke WW, Sherk HH. Normal adult anatomy. In: Sherk HH, editor. The cervical spine. Philadelphia: JB Lippincott; 1989. p. 11.
14. Yenerich DO, Haughton VM. Oblique plane MR imaging of the cervical spine. J Comput Assist Tomogr 1986;10:823.
15. Modic MT, Masaryk TJ, Ross JS, et al. Cervical radiculopathy: value of oblique MR imaging. Radiology 1987;163:227.
16. Drake RL, Vogl AW, Mitchell AW, et al. Gray's atlas of anatomy. Philadelphia: Churchill Livingstone; 2007.
17. Boden S, Davis D, Dina T, et al. Abnormal magnetic resonance scans of the lumbar spine in asymptomatic subjects: a prospective investigation. J Bone Joint Surg Am 1990;72:403–8.
18. Yu S, Haughton V, Sether LA. Anulus fibrosus in bulging intervertebral disks. Radiology 1988;169: 761–3.
19. Jensen M, Brant-Zawadski M, Obuchowski N, et al. Magnetic resonance imaging of the lumbar spine in people without back pain. N Engl J Med 1995;331: 69–73.
20. Dooms GC, Fisher MR, Hricack H, et al. Bone marrow imaging: magnetic resonance studies related to age and sex. Radiology 1985;155:429–32.
21. Reicher MA, Gold RH, Halbach VV, et al. MR imaging of the lumbar spine: anatomic correlations and the effects of technical variations. Am J Roentgenol 1986;147:891–8.
22. Czervionke LF, Daniels DL, Ho PSP, et al. Cervical neural foramina: correlative anatomic and MR imaging study. Radiology 1988;169:753.
23. Czervionke LF, Daniels DL, Ho PSP, et al. The MR appearance of gray and white matter in the cervical spinal cord. AJNR Am J Neuroradiol 1988;9:557–62.
24. Loevner L, Tobey JD, Yousem DM. MR imaging characteristics of cranial bone marrow in adult patients with underlying systemic disorders compared with healthy control subjects. AJNR Am J Neuroradiol 2002;23(2):248–54.
25. Ricci C, Cova M, Kang YS, et al. Normal age-related patterns of cellular and fatty bone marrow distribution in the axial skeleton: MR imaging study. Radiology 1990;177:83–8.
26. Eito K, Waka S, Naoko N, et al. Vertebral neoplastic compression fractures: assessment by dual-phase chemical shift imaging. J Magn Reson Imaging 2004;20:1020–4.
27. Baker LL, Goodman SB, Perkash I, et al. Benign versus pathologic compression fractures of vertebral

bodies: assessment with conventional spin-echo, chemical-shift, and STIR MR imaging. Radiology 1990;174:495–502.

28. Erly WK, Oh ES, Outwater EK. The utility of in-phase/opposed-phase imaging in differentiating malignancy from acute benign compression fractures of the spine. AJNR Am J Neuroradiol 2006; 27:1183–8.
29. Pomerantz SI. Myelography: modern techniques and indications. In: Masdeu JC, Gilberto González R, editors. Handbook of clinical neurology. Amsterdam: Elsevier; 2016. p. 193–208.
30. Hoeffner EG, Mukherji SK, Srinivasan A, et al. Neuroradiology back to the future: head and neck imaging. AJNR Am J Neuroradiol 2012; 33(11):2026–32.
31. Schmorl G, Junghanns H. The human spine in health and disease. NewYork: Grune and Stratton; 1959. p. 12.
32. Laredo JD, Reizine D, Bard M, et al. Vertebral hemangiomas: radiologic evaluation. Radiology 1986; 161:183.
33. Bronskill MJ, McVeigh ER, Kucharazyk W, et al. Syrinx-like artifacts on MR images of the spinal cord. Radiology 1988;166:485–8.
34. Bellon EM, Haacke EM, Coleman PE, et al. MR artifacts: a review. Am J Roentgenol 1986;147:1271–81.
35. Pusey E, Lufkin R, Brown R, et al. Magnetic resonance imaging artifacts: mechanisms and clinical significance. Radiographics 1986;6:891–911.
36. Czervionke LF, Czervionke JM, Daniels DL, et al. Characteristic features of MR truncation artifacts. AJNR Am J Neuroradiol 1988;9:815–24.